# Schroedinger Eigenmaps for the Analysis of Bio-Medical Data

Wojciech Czaja and Martin Ehler

arXiv:1102.4086v2 [cs.CE] 26 Sep 2012

***Abstract*—We introduce Schroedinger Eigenmaps, a new semi-supervised manifold learning and recovery technique. This method is based on an implementation of graph Schroedinger operators with appropriately constructed barrier potentials as carriers of labeled information. We use our approach for the analysis of standard bio-medical datasets and new multispectral retinal images.**

***Index Terms*—Schroedinger Eigenmaps, Laplacian Eigenmaps, Schroedinger operator on a graph, barrier potential, dimension reduction, manifold learning.**

## I. Introduction

Typical modern bio-medical data are characterized by high complexity (usually by means of high dimensionality), and the underlying nonlinear processes are often unknown, forming a fundamental barrier to better understand human physiology. Moreover, as personalized medicine expands, increasingly detailed patient data need to be integrated in clinical trials and individual treatment decisions, which usually results in a complicated classification problem.

Data driven analysis schemes are commonly based on kernels that derive the proper classification directly from the data. However, bio-medical applications are also characterized by low signal to noise ratio so that effective schemes require additional expert input. This outside information is, depending on the perspective, called labeling, (semi-) supervision, regularization, or learning from training data. Often, because of the nature of medical experiments, there are only few training points available and analysis schemes are needed that learn from these few data points most efficiently, while being robust against perturbations.

Examples of kernel based analysis techniques are Locally Linear Embedding (LLE) [37], Hessian-based LLE [23], Laplacian Eigenmaps [4], Diffusion Wavelets [17], [18], or Diffusion Maps [16], and kernel PCA and Support Vector Machines [39]. These methods represent the data in form of a graph, with nodes that are formed by the data vectors, and with edges that represent the distances between pairs of such vectors. This information is stored in the adjacency matrix, which then is modified to form the kernel.

W. Czaja is with University of Maryland, Department of Mathematics, College Park, MD 20742, wojtek@math.umd.edu.

M. Ehler is with Helmholtz Zentrum München, German Research Center for Environmental Health, Institute of Biomathematics and Biometry, Ingolstädter Landstr. 1, D-85764 Neuherberg, martin.ehler@helmholtz-muenchen.de. He is also with National Institutes of Health, Eunice Kennedy Shriver National Institute of Child Health and Human Development, Section on Medical Biophysics, 9 Memorial Drive, Bethesda, MD 20892, ehlermar@mail.nih.gov.

Physical or experimental constraints often suggest that the data points belong to a low-dimensional manifold. Many kernel-based methods recover this manifold by means of representations in terms of the most significant eigenvectors of the kernel matrix [42]. A major feature of Laplacian Eigenmaps and related methods is the preservation of local spectral distances, while reducing the overall dimension of the data represented by the aforementioned graph, cf., [15]. It has been successfully applied to pattern recognition and segmentation problems [40], [46] and [2], [8].

Laplacian Eigenmaps and similar methods originally lead to fully automated classification algorithms but have also been modified to work in semi-supervised settings: Belkin and Niyogi [3], [5], for instance, proposed to use classifiers induced from partially labelled data on the Laplacian representation of unlabeled points. Belkin et al. [7] used regularization in reproducing kernel Hilbert spaces to obtain a family of semi-supervised and transductive learning algorithms related to Laplacian Eigenmaps. In [35], extensions of the regularization methods proposed in [7] are obtained via inverse regression. In related developments, Zhu et al. [49] proposed to augment the data graph with the results of a prior classifier. Local discriminant analysis to locally modify ("warp") the diffusion metric is proposed by Coifman et al. in [17]. Szlam et al. [41] developed a further generalization by means of collecting all the class information into a modification of the metric used to build the kernel.

In the present paper we develop a new *Schroedinger Eigenmaps algorithm* that builds upon Laplacian Eigenmaps and steers the diffusion process within the uniform theory of Schroedinger operators in place of the Laplacian. Experts (e.g., trained practitioners) can introduce their input in form of a barrier potential for the associated Schroedinger operator on a graph to improve the detection and classification processes by steering the Schroedinger diffusion process effectively. At the same time, the new graph Schroedinger operator converges towards the Schroedinger operator on the manifold (just like the Laplacian kernel converges towards the Laplace-Beltrami operator), see Section III-B.

Such defined barrier Schroedinger potentials are easy to implement and appear in our numerical experiments to be well-suited for the analysis of low quality data with only few training points available – a typical situation in bio-medical applications. After having validated the usefulness of Schroedinger Eigenmaps (SE) by comparison to Support Vector Machines (SVM) on three standard medical datasets,

we apply our method to analyze multispectral retinal images and genetic expression profiles. The proposed scheme provides two major features for data segmentation. On one hand, by an appropriate selection of the potential, it allows the practitioner to separate data vectors, which should not appear in the same class. Specifically, in bio-medical imaging, the practitioner could be a physician who has additional information from results of other imaging devices or from physiological processes and knowledge about disease progression. On the other hand, Schroedinger Eigenmaps allow to identify complex regions by means of decreasing the relative distances between labeled representatives. For the physician who has already identified several different regions of pathology, this technique allows to collect these regions into one pathology class and therefore allows to better indentify normal physiology.

In Section II we review Laplacian Eigenmaps. We introduce the new Schroedinger Eigenmaps with an investigation of its properties in Section III, where we also visualize the behavior on artificial data. Section III-E is dedicated to the description of the intertwining of Schroedinger Eigenmaps and classification schemes. In Section IV, we compare Schroedinger Eigenmaps with Support Vector Machines on 3 standard medical datasets. We also analyze new multispectral retinal images.

## II. Laplacian Eigenmaps

Given $m$ points $\{x_1, \dots, x_m\} \subset \mathbb{R}^N$, we assume that they belong to an $n$-dimensional manifold, where $n$ is much smaller than $N$. The goal is to recover this manifold or, in other words, to find a low-dimensional representation $\{y_1, \dots, y_m\} \subset \mathbb{R}^n$ of the original dataset $\{x_1, \dots, x_m\} \subset \mathbb{R}^N$. Here, we briefly recall the three-step procedure of Laplacian Eigenmaps, see [4]:

**Step 1.** *Adjacency graph construction:*
Build a graph $\mathcal{G}$, whose nodes $i$ and $j$ are connected if $x_i$ is among the $k$-nearest neighbors of $x_j$ or vice versa. The distances between data points are measured in the Euclidean metric. The graph $\mathcal{G}$ represents the connectivity of the data, and $k$ is a parameter.

**Step 2.** *Heat kernel as weights:*
Weight the edges of the graph. A typical example is the *diffusion weight matrix* $W$ given by

$$W_{i,j} = \begin{cases} e^{-\frac{\|x_i - x_j\|^2}{\sigma}}, & i \text{ and } j \text{ are connected,} \\ 0, & \text{otherwise.} \end{cases}$$

**Step 3.** *Solving an eigenvalue problem:*
Let $D$ be a diagonal matrix with $D_{i,i} = \sum_j W_{i,j}$. Denote the low-dimensional representation by an $m \times n$ matrix $y = (y_1, \dots, y_m)^\top$, where each row $y_i$ is considered as a vector in $\mathbb{R}^n$. Next, consider the following minimization problem

$$\min_{y^\top D y = I} \tfrac{1}{2} \sum_{i,j} \|y_i - y_j\|^2 W_{i,j} = \min_{y^\top D y = I} \operatorname{trace}(y^\top L y), \tag{1}$$

where $L = D - W$ is the $m \times m$ Laplace operator and $I$ is the identity matrix. The minimizer of (1) is given by the $n$ minimal eigenvalue solutions of $Lx = \lambda D x$ under the constraint $y^\top D y = I$, i.e., the columns of the minimizer $y^{(0)}$ are the $n$ eigenvectors with respect to the smallest eigenvalues. If the graph is connected, then $\mathbf{1} = (1, \dots, 1)^\top$ is the only eigenvector with eigenvalue 0. Instead of (1), we solve for $\min \operatorname{trace}(y^\top L y)$ subject to $y^\top D y = I$, $y^\top D^{1/2} \mathbf{1} = 0$. By applying $z = D^{1/2} y$, this yields $\min \operatorname{trace}(z^\top \mathcal{L} z)$ subject to $z^\top z = I$, $z^\top \mathbf{1} = 0$, where $\mathcal{L} = D^{-1/2} L D^{-1/2}$. The minimizer $z^{(0)}$ is given by the $n$ eigenvectors with smallest nonzero eigenvalue, and we obtain the sought $n$-dimensional representation $\{y_1, \dots, y_m\}$ from $y = D^{-1/2} z^{(0)}$.

Though algorithms based on spectral decomposition, such as Laplacian Eigenmaps, provide a powerful tool for non-linear dimensionality reduction and manifold learning, they are not without certain shortcomings. We refer the interested reader to, e.g., [28], [29], [43].

## III. Schroedinger Eigenmaps

The idea of using solutions of the Laplace equation for labeling is not new. In [30], for instance, the concept is utilized for image segmentation, where a small number of pixels is labeled, and random walk theory is then applied to classify unlabeled surrounding pixels. We aim to develop a more general classification framework by means of Schroedinger operators. This approach allows for more flexible labeling schemes. Moreover, a significant advantage of the Schroedinger Eigenmaps technique is that it applies not just to surrounding pixels, but to any image location allowing for classes whose members are not spatially connected. This more general approach enables its application to data that do not encode location as, for instance, gene expressions.

The motivation behind this approach is two-fold. Mathematically, we are interested in shifting the analysis of complex, high-dimensional phenomena towards studying the associated operators acting on these data-dependent graphs, and away from analyzing pointwise relationships between the graph nodes. Physically, partially labeled sets naturally lead to the notion of barrier potentials and to the way in which these potentials affect the diffusion processes on graphs. As such, by appropriately choosing locations of the potential barriers we can steer the diffusion process to allow for identification of the correct cluster containing the labels, when compared to unobstructed diffusion process of the Laplacian Eigenmaps algorithm.

We would like to point out that [1] and [11] deal with Schroedinger equations with Hamiltonians, which are Laplacians without any potential. We, on the other hand, deal with Schroedinger operators, which are Laplacians with barrier potentials; as such, these are two different generalizations of the Laplace operator approach.

### A. From Laplace to Schroedinger

The matrices $L$ and $\mathcal{L}$ in the previous section can be associated with the notion of the Laplace operator $\Delta$,

cf. [4]. The related diffusion equation $\partial_t \varphi = \Delta \varphi$ is extended to the Schroedinger Equation

$$\partial_t \psi(x,t) = \Delta \psi(x,t) + v(x)\psi(x,t) \tag{2}$$

by adding a potential term $v(x)$ to the Laplace operator. We revisit this idea in the following section to introduce a discrete Schroedinger operator.

### B. Schroedinger Eigenmaps

The potential $v$ in (2) is considered as a nonnegative multiplier operator. The discrete analogue of $\mathcal{E} = \Delta + v$ is the matrix $E = L + V$, where $V$ is a nonnegative diagonal $m \times m$ potential matrix. We replace (1) with

$$\min_{y^\top D y = I} \operatorname{trace}(y^\top (L + \alpha V) y), \tag{3}$$

which is equivalent to

$$\min_{y^\top D y = I} [\operatorname{trace}(y^\top L y) + \operatorname{trace}(y^\top \alpha V y)].$$

The parameter $\alpha \geq 0$ is added here so that it can be used to emphasize the relative significance of the potential $V$ with respect to the graph Laplace operator.

According to (1), the minimization problem (3) is equivalent to

$$\min_{y^\top D y = I} \tfrac{1}{2} \sum_{i,j} \|y_i - y_j\|^2 W_{i,j} + \alpha \sum_i V(i) \|y_i\|^2, \tag{4}$$

where $V = \operatorname{diag}(V(1), \ldots, V(m))$. The first component of the above sum incurs a penalty, when neighboring points $x_i$ and $x_j$ are mapped into points $y_i$ and $y_j$, respectively, which are far apart. The second component penalizes these points $y_i$, $i = 1, \ldots, m$, which are associated with large values of $V(i)$. Alternatively speaking, if $V$ took only two values, 0 and 1, then the minimization (4) yields a dimension-reduced representation $y$, which forces increased clustering of the representations $y_i$ of points associated with the value $V(i) = 1$, while attempting to ensure that close points remain close after the dimension reduction. As such we may utilize the potential $V$ to *label* points which we want to be identified together after the dimension reduction. Because of the built-in preservation of topology of the point cloud (induced by the Laplacian), this labeling may be used to segment a particular class of points. We shall make this intuition clear in the following sections, see, e.g., Corollary III.2 and Corollary III.4, or the applications in Section IV.

It is known that the (rescaled) graph Laplacian converges towards the Laplace-Beltrami operator on the underlying manifold, e.g., [6], [44]. This convergence carries over to the Schroedinger operator as we shall see next. The Laplacian map is given by

$$L_m^\sigma f(x_i) = f(x_i) \sum_j e^{-\frac{\|x_i - x_j\|^2}{\sigma}} - \sum_j f(x_j) e^{-\frac{\|x_i - x_j\|^2}{\sigma}}.$$

For the purpose of this analysis we choose $k = m$, i.e., we assume that all data points are connected. Replacing the $x_i$ by an arbitrary $x \in \mathbb{R}^n$ yields the extension to $\mathbb{R}^d$:

$$L_m^\sigma f(x) = f(x) \sum_j e^{-\frac{\|x - x_j\|^2}{\sigma}} - \sum_j f(x_j) e^{-\frac{\|x - x_j\|^2}{\sigma}}.$$

It turns out that there exists a positive constant $C$ such that for i.i.d. uniformly sampled data points $\{x_1, \ldots, x_m\}$ and $\sigma_m = 4m^{-\frac{1}{n+2+s}}$, where $s > 0$, and $f \in \mathcal{C}^\infty(\mathcal{M})$, we have the convergence

$$\lim_{m \to \infty} C \frac{(\pi \sigma_m)^{-\frac{n+2}{2}}}{m} L_m^{\sigma_m} f(x) = \Delta_{\mathcal{M}} f(x) \tag{5}$$

in probability, cf. [6]. Let $v$ be a given potential on the manifold $\mathcal{M}$. The associated matrix $V$ acting on a discrete $m$-point cloud is defined as $V = \operatorname{diag}(v(x_1), \ldots, v(x_m))$. Since the potential does not depend on $\sigma$, we may replace $x_i$ by an arbitrary $x \in \mathbb{R}^n$ to obtain the map:

$$V_m f(x) = v(x) f(x).$$

Clearly this extension coincides with the continuous potential on the manifold. As such, adding the discrete potential $V_m$ to the discrete Laplacian does not impede the convergence in (5). Consequently, the term

$$C \frac{(\pi \sigma_m)^{-\frac{n+2}{2}}}{m} L_m^{\sigma_m} f(x) + V_m f(x) \tag{6}$$

converges for $n \to \infty$ towards

$$\Delta_{\mathcal{M}} f(x) + v(x) f(x)$$

in probability. For more results on convergence of the Schroedinger Eigenmaps algorithm to Schroedinger operators on manifolds, we refer the interested reader to [33] and [20].

We close this section by noting that expression (6) induces a specific choice of the parameter $\alpha$. Indeed, in order to consider $E = L + \alpha V$, rescaling of $L_m^{\sigma_m}$ in (6) implies the need to reversely rescale $V$. This can be done by means of multiplication with $\alpha = \frac{1}{C} \frac{m}{(\pi \sigma_m)^{-\frac{n+2}{2}}}$, which tends to infinity as $m \to \infty$. As such, optimal selection of $\alpha$ is related to the size of the dataset.

### C. General Properties

In this section we study the properties of the Schroedinger Eigenmaps (SE). We shall see that the potential can be used to push vectors towards zero, which can be helpful in classification tasks. In fact, we shall see later that even nondiagonal "potentials" make sense and, thus, address a more general setting where $E = L + \alpha V$ is symmetric positive semi-definite. Note that $E$ can still be diagonalized and all eigenvalues are nonnegative. If $V \neq 0$ is a nonnegative diagonal potential, then $\mathbf{1} \notin \operatorname{null}(V)$. For a connected graph $\mathcal{G}$, the latter implies that $E = L + \alpha V$ has full rank, i.e., there is no eigenvalue that equals zero.

To study the effect of the potential $V$ on eigenvectors of the Schroedinger operator, we make use of the notation $\|y\|_M^2 := \operatorname{trace}(y^\top M y)$ for a matrix $M$ and we denote $\mathcal{V} := D^{-1/2} V D^{-1/2}$:

**Theorem III.1.** *Let $V$ be symmetric positive semi-definite, $n \leq \dim(\operatorname{null}(V))$, and let $y^{(\alpha)}$ be a minimizer of* (3)*.*

a) *There is a constant $C_1 \geq 0$ such that*

$$\|y^{(\alpha)}\|_V^2 \leq C_1 \frac{1}{\alpha}. \tag{7}$$

b) *If $z_{\text{null}}^{(\alpha)}$ is the columnwise orthogonal projection of $z^{(\alpha)} = D^{1/2}y^{(\alpha)}$ onto $\text{null}(\mathcal{V}) \neq \{0\}$, then there is a constant $C_2 \geq 0$ such that*

$$\|z_{\text{null}}^{(\alpha)}\|_I^2 \geq n - C_2\frac{1}{\alpha}. \tag{8}$$

*Proof:* First, we address part (a). Applying $z = D^{1/2}y$ to (3) yields

$$\min_{z^\top z = 1} \text{trace}(z^\top(\mathcal{L} + \alpha\mathcal{V})z). \tag{9}$$

Since $\mathcal{V}$ is symmetric, (9) can be rewritten as

$$\min_{\substack{z_{\text{null}} \in \text{null}(\mathcal{V}),\, z_{\text{null}}^\perp \in \text{null}(\mathcal{V})^\perp \\ z = z_{\text{null}} + z_{\text{null}^\perp},\, z^\top z = I}} \text{trace}(z^\top \mathcal{L} z + z_{\text{null}^\perp}^\top \alpha\mathcal{V} z_{\text{null}^\perp}),$$

where $z_{\text{null}}$ is a matrix whose columns are contained in $\text{null}(\mathcal{V})$. The constant

$$C_1 := \min_{\substack{z_{\text{null}}^\top z_{\text{null}} = I \\ z_{\text{null}} \in \text{null}(\mathcal{V})}} \text{trace}(z_{\text{null}}^\top \mathcal{L} z_{\text{null}})$$

only depends on the nullspace of $\mathcal{V}$, and it is associated with the choice $z_{\text{null}^\perp} = 0$. Since $y^{(\alpha)}$ is a minimizer of (3), $z^{(\alpha)} = D^{1/2}y^{(\alpha)}$ is a minimizer of (9). Obviously, we have $\|z^{(\alpha)}\|_{\mathcal{L}}^2 + \|z^{(\alpha)}\|_{\alpha\mathcal{V}}^2 \leq C_1$, and according to $\|z^{(\alpha)}\|_{\mathcal{L}}^2 \geq 0$, we obtain $\|z^{(\alpha)}\|_{\alpha\mathcal{V}}^2 \leq C_1$. This finally yields $\|z^{(\alpha)}\|_{\mathcal{V}}^2 \leq C_1\frac{1}{\alpha}$. Since $\|z^{(\alpha)}\|_{\mathcal{V}}^2 = \|y^{(\alpha)}\|_V^2$, we have proven (7).

In order to verify (8), we will use

$$z^{(\alpha)^\top}_{\text{null}} z^{(\alpha)}_{\text{null}} = I - z^{(\alpha)^\top}_{\text{null}^\perp} z^{(\alpha)}_{\text{null}^\perp}.$$

Note that $\mathcal{V}$ is symmetric positive semi-definite and therefore $\|\cdot\|_{\mathcal{V}}$ is a norm on $\text{null}(\mathcal{V})^\perp$. Since all norms on a finite dimensional vector space are equivalent, there is a constant $C > 0$ such that $\|\cdot\|_I \leq C\|\cdot\|_{\mathcal{V}}$ on $\text{null}(\mathcal{V})^\perp$. By applying $C_2 := C^2C_1$, we get the estimate

$$\begin{aligned}\|z_{\text{null}}^{(\alpha)}\|_I^2 &= n - \|z_{\text{null}^\perp}^{(\alpha)}\|_I^2 \geq n - C^2\|z_{\text{null}^\perp}^{(\alpha)}\|_{\mathcal{V}}^2 \\ &= n - C^2\|z^{(\alpha)}\|_{\mathcal{V}}^2 = n - C^2\|y^{(\alpha)}\|_V^2 \\ &\geq n - C_2\frac{1}{\alpha}.\end{aligned}$$

■

Let us now state the consequences of Theorem III.1 for a diagonal potential $V$.

**Corollary III.2.** *Under the assumptions and notation of Theorem* III.1*, let $V = \text{diag}(v_1, \ldots, v_m)$, then we have, for all $i = 1, \ldots, m$,*

$$v_i\|y_i^{(\alpha)}\|^2 \leq \sum_{i=1}^m v_i\|y_i^{(\alpha)}\|^2 = \|y^{(\alpha)}\|_V^2 \leq C_1\frac{1}{\alpha}.$$

**Remark III.3.** Let $V = \text{diag}(1, 0, \ldots, 0)$, then $y_1^{(\alpha)}$ is pushed to zero according to Corollary III.2. If $x_1$ and $x_2$ were sufficiently close, then we expect that $y_2^{(\alpha)}$ is also pushed to zero due to the linkage induced by $L$.

Corollary III.2 means that a diagonal potential pushes entries of $y^{(\alpha)}$ to zero. On the other hand, the potential does not force any collapse:

**Corollary III.4.** *Under the assumptions and notation of Theorem* III.1*, let $V = \text{diag}(v_1, \ldots, v_m)$.*

a) *If $v_1, \ldots, v_r \neq 0$ and $v_{r+1}, \ldots, v_m = 0$, then*

$$\sum_{i=r+1}^m D_{i,i}\|y_i^{(\alpha)}\|^2 \geq n - \max_{i=1,\ldots,r}\{\tfrac{D_{i,i}}{v_i}\}C_1\frac{1}{\alpha}.$$

b) *If $v_1 = D_{1,1}, \ldots, v_r = D_{r,r}$ and $v_{r+1}, \ldots, v_m = 0$, then*

$$\sum_{i=r+1}^m v_i\|y_i^{(\alpha)}\|^2 \geq n - C_1\frac{1}{\alpha}.$$

*Proof:* Part (b) is a special case of part (a). To prove part (a), we apply Corollary III.2, which yields

$$\begin{aligned}\sum_{i=r+1}^m D_{i,i}\|y_i^{(\alpha)}\|^2 &= \sum_{i=r+1}^m \|z_i^{(\alpha)}\|^2 = \|z_{\text{null}}^{(\alpha)}\|_I^2 \\ &= n - \|z_{\text{null}^\perp}^{(\alpha)}\|_I^2 = n - \sum_{i=1}^r D_{i,i}\|y_i^{(\alpha)}\|^2 \\ &\geq n - \sum_{i=1}^r \frac{D_{i,i}}{v_i}v_i\|y_i^{(\alpha)}\|^2 \\ &\geq n - \max_{i=1,\ldots,r}\{\tfrac{D_{i,i}}{v_i}\}\sum_{i=1}^r v_i\|y_i^{(\alpha)}\|^2 \\ &\geq n - \max_{i=1,\ldots,r}\{\tfrac{D_{i,i}}{v_i}\}C_1\frac{1}{\alpha}.\end{aligned}$$

■

Corrollary III.2 says that penalized locations are pushed to zero, and Corollary III.4 ensures that not all unlabeled data are collapsed into zero. Thus, labeling can lead to a separation between labeled and certain unlabeled data.

### *D. Schroedinger Eigenmaps: Nondiagonal Potentials*

While a diagonal potential $V$ is used to overweight or underweight certain nodes $y_i$, it turns out that nondiagonal "potentials" are useful as well. For $i \neq j$, let $V^{(i,j)}$ be the matrix with entries $V_{i,i}^{(i,j)} = V_{j,j}^{(i,j)} = 1$ and $V_{i,j}^{(i,j)} = V_{j,i}^{(i,j)} = -1$ and zeros elsewhere. One then verifies that

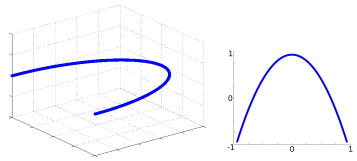
$$\text{trace}(y^\top \alpha V y) = \alpha\|y_i - y_j\|^2,$$

and Theorem III.1 yields

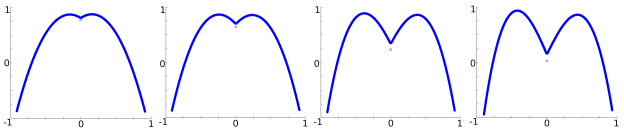
$$\|y_i^{(\alpha)} - y_j^{(\alpha)}\|^2 \leq C_1\frac{1}{\alpha}.$$

In other words, this kind of potential allows to identify points. Adding the matrix $V^{(i,j)}$ to the Laplacian has the flavor of modifying the underlying graph $\mathcal{G}$ by reweighting its edges. It allows for modifying the weights $W_{i,j}$, $i \neq j$, and we are able to penalize distances between data points which are not neighbors. We note that a similar change in the graph structure results from warping or weighted diffusion as proposed e.g., in [17] or [41].

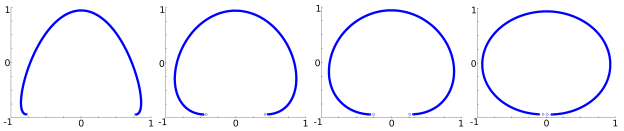
**Remark III.5.** If the graph $\mathcal{G}$ is connected, then $E = L + \alpha V^{(i,j)}$ has a simple eigenvalue equals zero since $\mathbf{1} \in \text{null}(V^{(i,j)})$. Thus, we should use the constraint $y^\top D^{1/2}\mathbf{1} = 0$ for SE with potentials $V^{(i,j)}$. To establish a



(a) (left) Original arc in three-dimensional space. (right) Laplacian Eigenmaps perfectly recovers the two-dimensional structure.



(b) The Schroedinger Eigenmaps with diagonal potential $V = \mathrm{diag}(0,\ldots,0,1,0,\ldots,0)$ only acting in one point $y_{i_0}$ in the middle of the arc for $\alpha = 0.05, 0.1, 0.5, 5$. This point is pushed to zero. Since $V$ is 'discontinuous', the dimension reduced arc gets more and more discontinuous until $y_{i_0}$ will become zero for sufficiently large $\alpha$. Then the arc does not deform any more.



(c) By labeling the end points of the arc within the nondiagonal potential $V^{(i,j)}$, for $\alpha = 0.01, 0.05, 0.1, 1$, we are able to control the dimension reduction such that we obtain an almost perfect circle (up to a small discontinuity).

Fig. 1. Schroedinger Eigenmaps applied to an arc

uniform methodology of Schroedinger Eigenmaps, we use the constraint $y^\top D^{1/2} w = 0$ throughout, where $w$ is an eigenvector of the Schroedinger operator $E = L + \alpha V$, with respect to the smallest eigenvalue. Thus, as in the case of Laplacian Eigenmaps, we skip the smallest eigenvectors and take the $n$ subsequent ones.

To demonstrate the use of the barrier potential, SE is applied to a three-dimensional arc in Figure 1.

**Remark III.6.** For the purpose of sequentially identifying points, we propose to use the potential

$$V = \sum_{i=1}^{m-1} V^{(i,i+1)}, \tag{10}$$

which penalizes $L$ by $\sum_{i=1}^{m-1} \|y_i - y_{i+1}\|^2$. Note that the eigenvectors of this matrix are the basis vectors of the discrete cosine transform of type II.

### *E. Schroedinger Eigenmaps For Classification*

In this section we discuss the standard Vector Angle Classification (VAC) in combination with Schroedinger Eigenmaps. In this regard, suppose we have $s$ pairwise different seed vectors $a_1, \ldots, a_s \in \mathbb{R}^n$, which represent the centers of each class. The class $C_i$ consists of $y_i^{(\alpha)}$s whose angle is closest to the specific center vector as long as the angle is smaller than some tightness parameter $\delta_i$. We additionally apply a threshold parameter $\delta$ to refuse $y_i^{(\alpha)}$s that have small norm, which by themself form another class.

According to Corollary III.2, SE can be applied to "force" processed pixels to zero at the rate $1/\sqrt{\alpha}$ and, hence, below any threshold $\delta > 0$ for sufficiently large $\alpha$. A practitioner can use labels in the form of a diagonal potential to separate a particular region of an image, see Section IV-B. On the other hand, different spatial regions can be identified with each other by labelling them with non-diagonal potentials $V^{(i,j)}$, cf., (10). This is useful to classify pathological areas as one single class despite the fact that intrinsic intra-class variations can be large.

As it was mentioned in the introduction, a very considerable effort has been aimed at developing partially labeled classification schemes based on the Laplacian Eigenmaps algorithm, on related graph random walks, or on Diffusion Maps. The classification scheme based on Schroedinger Eigenmaps with partially labeled data is novel. When compared to "warping" and function adapted diffusion processes [17] [41], Schroedinger Eigenmaps result in a more general class of matrices (operators), by allowing modifications to the diagonal as well as to the off-diagonal terms. These diagonal terms, in turn, are associated with locations of the barrier potential which affects and steers the diffusion process. On the other hand, Schroedinger Eigenmaps classification is a joint optimization process for labeled and unlabeled data, as opposed to classical semi-supervised algorithms [3], [5].

## IV. Biomedical Applications

The performance of Schroedinger Eigenmaps on three standard medical datasets is compared with linear and Gaussian kernel Support Vector Machines (SVM). After having verified the usefulness of Schroedinger Eigenmaps, we apply them to analyze new problems in genetic expression analysis and retinal multispectral imaging.

### *A. Three standard bio-medical datasets*

All 3 standard datasets are obtained from the UCI Machine Learning Repository. Training points are randomly selected. The potential is designed on the training data and SE are computed on the entire dataset so that VAC with threshold leads to the final class separation.

After removing missing values, the *Wisconsin Breast Cancer Database* (WBCD) [47] contains 683 patterns with 9 attributes and is grouped into two classes, benign and malignant. The diagonal potential is used on the benign class in the training data. The processed vectors that fall below a threshold form the predicted benign class on the entire dataset.

The *Cleveland Heart Disease Database* (CHDD) [22] contains 297 patterns with 13 attributes and is grouped into presence of heart disease (values 1,2,3,4) and absence (value 0). We removed 6 patterns due to missing values. Following the focus in the literature, we aim to separate absence from heart disease. We label absence in the training data using the diagonal potential and identify heart disease classes 1-4 by applying the nondiagonal potential. The

predicted absence class is formed by the vectors that fall below the threshold.

The *Mammographic Mass Data Set* (MMD) [27] contains $961$ instances and $5$ attributes that are grouped into benign and malignant. Note that we removed $131$ patterns due to missing values and suppressed the first attribute as it was a numerical assessment of the range between benign and malignant of a double-review process by physicians.

In our computations of SE, we keep $6$ eigenvectors, and the number of nearest neighbors varies between $6$ and $20$, the weight parameter $\alpha$ in the potential, and the threshold parameter are optimized for minimizing the error rates. We compare our method with Laplacian Eigenmaps (same parameters as for SE) and with SVM. The Matlab implementation of SVM is used with a linear and a Gaussian kernel function, and the separating hyperplane is found from least squares or a one-norm with soft-margin svm; the best result is taken. The parameter in the SVM Gaussian kernel corresponds to $\sigma$ in Schroedinger Eigenmaps. After optimization of $\sigma$ in SVM for each dataset separately, it appeared consistent that best results for both, SVM and SE, were obtained by choosing $\sigma = 1/2, 1, 2$ in SE and $2\sigma$ in SVM for the datasets WBCD, CHDD, and MMD, respectively.

Error rates for large training data yield information on the nonlinear data structure. For instance, as the error of the linear SVM applied to WBCD with $600$ training points does not vanish, the data cannot be separated in a linear fashion, see Table I.

The comparison to Laplacian Eigenmaps (same parameters as for Schroedinger Eigenmaps) shows how the potential can improve the classification process. If there are only few training data, then Schroedinger Eigenmaps lead to the smallest error rates among all methods, most considerably for CHDD and MMD. When increasing the number of training points, the Gaussian kernel SVM yields the best results except for MMD. Typical bio-medical data allow for only few reliable training data and in this situation Schroedinger Eigenmaps appear most useful.

| dataset, #training data | LE | SVM lin. | SVM Gauss. | SE |
|---|---|---|---|---|
| WBCD, 40 | 14% | 5% | 5% | 4% |
| WBCD, 100 | 9% | 4% | 4% | 3% |
| WBCD, 200 | – | 4% | 3% | 3% |
| WBCD, 400 | – | 4% | 2% | 3% |
| WBCD, 600 | – | 4% | 2% | 3% |
| CHDD, 40 | 42% | 21% | 19% | 15% |
| CHDD, 100 | – | 17% | 15% | 12% |
| CHDD, 200 | – | 16% | 11% | 12% |
| CHDD, 297 | – | 15% | 9% | 11% |
| MMD, 20 | 45% | 24% | 24% | 22% |
| MMD, 30 | 40% | 22% | 22% | 21% |
| MMD, 40 | 38% | 22% | 21% | 20% |
| MMD, 100 | – | 21% | 20% | 20% |
| MMD, 200 | – | 20% | 19% | 20% |
| MMD, 800 | – | 20% | 18% | 20% |

TABLE I
ERROR RATES AS INCORRECTLY CLASSIFIED SAMPLES / TOTAL DATA ARE AVERAGED OVER 100 INSTANCES FOR EACH METHOD. LE IS COMBINED WITH VAC, WHERE TRAINING DATA ARE USED AS SEEDS THAT ALWAYS END UP IN THE CORRECT CLASS. THEREFORE, THE LE OUTCOME FOR LARGE TRAINING DATA IS NOT DUE TO THE LE METHOD

### *B. Applications to new biomedical data*

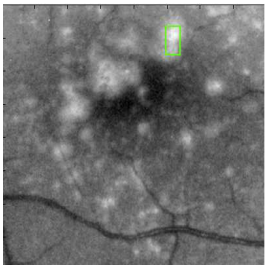
Up to this point we have compared Schroedinger Eigenmaps with other methods for semi-supervised classification. We believe the strength of our proposed technique is threefold: good performance with few labeled points, a global approach yielding good local discrimination, and ability to correctly classify in the presence of non-linear mixing. In this section we shall illustrate some of these points with two examples: a classification problem in medical imaging, and a clustering problem in genetic analysis. At the same time, these two examples give additional evidence for the results of the first part of our paper.

*1) Analysis of clinical, retinal images:* First, we analyze a problem in retinal imaging, where our goal is to detect and differentiate between two classes of chemical mixtures in the human retina. This problem is of interest to the medical community, as it appears in studies of age-related macular degeneration (AMD) – the leading cause of blindness among the elderly population in the developed world, see [14], [13], [19], [36]. The balance between these two chemical mixtures, which we want to detect, can be used to determine the stage of the disease and, in turn, the proper course of action [31], [32], [45]. There is demand in the medical community for automated analysis tools that enable detection and classification while, at the same time, allowing for expert input [24], [34], [38].

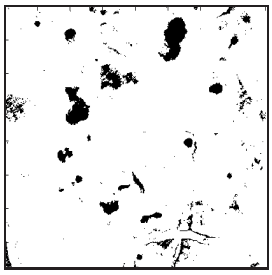
We shall apply our Schroedinger Eigenmaps technique, with the locations of the potential chosen by medical experts. This example further illustrates that relatively few (less than 0.1%) labels may lead to good classification results. An added difficulty in this scenario is that, due to limitations of the imaging device, the spectral information about the chemicals of interest is always nonlinearly mixed with various other responses, e.g., from layers just beneath the retina, or from different illumination patterns. As such, most of the mixing models that rely on presence of pure pixels in the image fail to work.

For each patient, 4 excitation with 2 emission filters and trifold imaging lead to $24$ images ($400 \times 400$ pixels) that are aligned by applying the commercial software i2k Align. One pixel, therefore, has $24$ entries in $z$-direction, so that the acquired dataset are $160000$ vectors in $24$-dimensional space. The earliest clinical signs of AMD are bright spots in retinal reflection images, see Fig. 2(a), referred to as *drusen* [9]. We have applied Schroedinger Eigenmaps with diagonal potential acting on a small predefined drusen area ($50$ pixels) that was identified by medical experts. The number of nearest neighbors was chosen to be $14$, $\sigma = 1$, $\alpha$ in the potential is $10$ times the average norm of the data vectors, and we used $15$ eigenvectors. We obtain a drusen map of all pixel vectors whose Schroedinger Eigenmaps coordinates fall below a threshold that was adjusted through visual inspection, cf. Fig. 2(b).

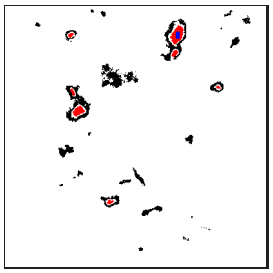
It was suggested in [21], that drusen centers may separate from outer drusen areas. To distinguish the two drusen



(a) drusen appear as bright spots; one is marked by the green square; detection and further subclassification is needed



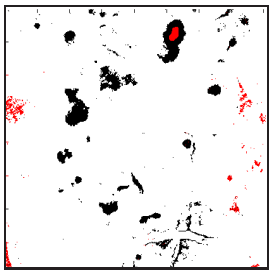
(b) only a small drusen region (50 pixels) in the upper left corner was penalized in the barrier potential providing one class of drusen



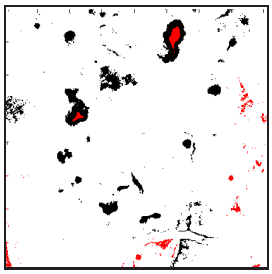
(c) blue area (75 pixels) was additionally identified by SE (non-diag. matrix); VAC with threshold yields 2 well-separated drusen classes (black/red). Consistent with [21], we separate drusen centers from outer drusen segments



(d) zoomed onto the marked drusen in (a); red lines show LRW segmentation; drusen center and outer drusen area were separated by using 3 sets of labels; drusen center (blue), drusen outer area (yellow), background (green)



(e) The class identified in (b) is further subclassified by running linear SVM on this subset with labels on the drusen center



(f) Gaussian SVM with labeled data as in (e) applied to the class in (b)

Fig. 2. Classification with Schroedinger Eigenmaps, LRW verification, and comparisons to SVM based on multi-spectral retinal image sets

subclasses, we additionally form a second potential on a drusen center (75 pixels) that identifies pixels and run SE simultaneously with both potentials activated. We obtain two subclasses of drusen, one by pixels whose Schroedinger Eigenmaps coordinates fall below the threshold, the other one is derived from taking the average over identified pixel vectors as a seed in VAC. Threshold and class tightness parameter are optimized through visual inspection, see Fig. 2(c). The same label locations are used for linear and Gaussian SVM that are applied to the detected drusen in Fig. 2(b) for further subclassification, see Fig. 2(e,f).

In a single drusen, members of the same class are spatially connected, so that we can apply the segmentation tool Laplacian Random Walk (LRW) in [30], confirming the drusen subclassification, cf. Fig. 2(d). SE appears well-suited to incorporate spatially unconnected regions, going beyond image segmentation.

*2) Analysis of gene expressions:* Recent efforts in biology focus on the understanding of genetic datasets based on complex gene interactions, rather than analyzing genes individually. This shift of perspectives increases the importance of small local variations, which may be irrelevant from a purely global perspective. Therefore, analysis and classification of time series gene expressions require the balance between local and global variations.

Hierarchical clustering in [12] and Laplacian Eigenmaps in [25] was used to tentatively analyze a collection of 8316 microarray gene expressions at 8 time-points related to eye morphology in mice, see [10], [48] for further background. The goal of those studies was to identify new gene clusters within this dataset that are associated to eye development.

We used a barrier potential in [26] to label certain DNA specific proteins (transcription factors) and found a set of new genes related to eye morphogenesis, which were not discovered by traditional hierachichal techniques. Thus, even a preliminary application of the barrier potential for data labeling proved useful in [26] to add complementary expert data enabling improvements in gene clustering.

## V. Conclusions

We have introduced a generalization of Laplacian Eigenmaps to allow for expert data in form of a potential on a data-dependent graph. The properties of our novel Schroedinger Eigenmaps are studied, and we illustrate their action on both, artificial and standard medical data. At this stage these are only illustrations, and providing mathematical formalism behind these results is part of our on-going and future work on this subject. It appears that our method is robust and particularly useful if the data quality is low and there are only few training data, a typical situation in bio-medical applications. In addition, our scheme is successfully applied to the analysis of retinal multispectral images. We classify drusen based on few training pixels that were labeled by a physician. Our results suggest that Schroedinger Eigenmaps are useful in high-dimensional bio-medical data analysis when limited expert knowledge is available.

## Acknowledgment

This work was supported by the Intramural Research Program of NICHD/NIH, by NSF (CBET0854233), by NGA (HM15820810009), by ONR (N000140910144), and by NIH/DFG (EH 405/1-1/575910). The authors also express their gratitude to Drs. R. F. Bonner, B. Brooks, E. Y. Chew, and S. M. Meyers for their assistance with acquiring and analyzing the included datasets. We also acknowledge V. N. Rajapakse and the anonymous referees for their valuable comments and suggestions that led to the improvement of this paper.

## REFERENCES


[1] M. Aubry, U. Schlickewei, and D. Cremers, "The wave kernel signature: A quantum mechanical approach to shape analysis," in *IEEE International Conference on Computer Vision*, 2011.

[2] C. M. Bachmann, T. L. Ainsworth, and R. A. Fusina, "Exploiting manifold geometry in hyperspectral imagery," *IEEE Trans. Geosci. Remote Sens.*, vol. 43, no. 3, pp. 441–454, 2005.

[3] M. Belkin and P. Niyogi, "Using manifold structure for partially labeled classification," in *NIPS*, 2002.

[4] ——, "Laplacian eigenmaps for dimensionality reduction and data representation," *Neural. Comput.*, vol. 15, no. 6, pp. 1373–1396, 2003.

[5] ——, "Semi-supervised learning on riemannian manifolds," *Machine Learning*, vol. 56, pp. 209–239, 2004.

[6] ——, "Towards a theoretical foundation for laplacian-based manifold methods," *J. Comput. System Sci.*, vol. 74, no. 8, pp. 1289–1308, 2008.

[7] M. Belkin, P. Niyogi, and V. Sindhwani, "Manifold regularization: A geometric framework for learning from labeled and unlabeled examples," *Journal of Machine Learning Research*, vol. 7, pp. 2399–2434, Nov. 2006.

[8] J. J. Benedetto, W. Czaja, J. C. Flake, and M. Hirn, "Frame based kernel methods for automatic classification in hyperspectral data," in *IEEE IGARSS*, Cape Town, South Africa, 2009.

[9] A. C. Bird and al., "An international classification and grading system for age-related maculopathy and age-related macular degeneration. The international ARM epidemiological study group." *Surv. Ophthalmol.*, vol. 39, no. 5, pp. 367–374, Mar-Apr 1995.

[10] R. F. Bonner and al., "Laser capture microdissection: molecular analysis of tissue," *Science*, vol. 21, no. 278, pp. 1481–1483, 1997.

[11] A. M. Bronstein, "Spectral descriptors for deformable shapes," *arXiv:1110.5015v1*, 2011.

[12] J. D. Brown and al., "Expression profiling during ocular development identifies 2 nlz genes with a critical role in optic fissure closure," *Proc. Nat. Acad. Sci. USA*, vol. 106, no. 5, pp. 1462–7, Feb 2009.

[13] E. Y. Chew and al., "Risk of advanced age-related macular degeneration after cataract surgery in the age-related eye disease study: Areds report 25," *Ophthalmology*, vol. 116, no. 2, pp. 297–303, Feb 2009.

[14] E. Y. Chew, A. S. Lindblad, T. Clemons, and Age-Related Eye Disease Study Research Group, "Summary results and recommendations from the age-related eye disease study," *Arch. Ophthalmol.*, vol. 127, no. 12, pp. 1678–9, Dec 2009.

[15] F. R. K. Chung, "Spectral Graph Theory," *CBMS Regional Conference Series in Mathematics*, vol. 92, 1997.

[16] R. R. Coifman and S. Lafon, "Geometric harmonics: A novel tool for multiscale out-of-sample extension of empirical functions," *Appl. Comput. Harmon. Anal.*, vol. 21, no. 1, pp. 31–52, 2006.

[17] R. R. Coifman, S. Lafon, A. B. Lee, M. Maggioni, B. Nadler, F. J. Warner, and S. W. Zucker, "Geometric diffusions as a tool for harmonic analysis and structure definition of data. part i: Diffusion maps," *Proc. Nat. Acad. Sci.*, vol. 102, pp. 7426–7431, 2005.

[18] R. R. Coifman and M. Maggioni, "Diffusion wavelets," *Appl. Comput. Harmon. Anal.*, vol. 21, no. 1, pp. 53–94, 2006.

[19] H. R. Coleman, C. Chan, F. L. Ferris, and E. Y. Chew, "Age-related macular degeneration," *Lancet*, vol. 372, no. 9652, pp. 1835–45, Nov 2008.

[20] W. Czaja and A. Halevy, "On convergence of schroedinger eigenmaps," *preprint*, 2011.

[21] F. C. Delori and al., "Autofluorescence distribution associated with drusen in age-related macular degeneration," *Invest. Ophthalmol. Vis. Sci.*, vol. 41, no. 2, pp. 496–504, 2000.

[22] R. Detrano and et al., "International application of a new probability algorithm for the diagnosis of coronary artery disease," *American Journal of Cardiology*, vol. 64, pp. 304–310, 1989.

[23] D. L. Donoho and C. Grimes, "Hessian eigenmaps: new locally linear embedding techniques for high-dimensional data," *Proc. Nat. Acad. Sci.*, vol. 100, pp. 5591–5596, 2003.

[24] M. Ehler, J. Dobrosotskaya, and al., "Modeling photo-bleaching kinetics to map local variations in rod rhodopsin density," *SPIE Medical Imaging, Computer-Aided Diagnosis*, vol. 7963, 2011.

[25] M. Ehler, V. N. Rajapakse, B. Zeeberg, B. Brooks, J. Brown, W. Czaja, and R. F. Bonner, "Analysis of temporal-spatial covariation within gene expression microarray data in an organogenesis model," in *6th International Symposium on Bioinformatics Research and Applications (ISBRA'10)*, ser. Lecture Notes in Bioinformatics. Springer Verlag, 2010.

[26] ——, "Nonlinear gene cluster analysis with labeling for microarray gene expression data in organ development," *BMC Proceedings*, vol. 5(Suppl 2), p. S3, 2011.

[27] M. Elter, R. Schulz-Wendtland, and T. Wittenberg, "The prediction of breast cancer biopsy outcomes using two CAD approaches that both emphasize an intelligible decision process," *Medical Physics*, vol. 34, no. 11, pp. 4164–4172, 2007.

[28] S. Gerber, T. Tasdizen, and R. Whitaker, "Robust non-linear dimensionality reduction using successive 1-dimensional laplacian eigenmaps," in *Proceedings of the 24th international conference on Machine learning*, 2007, pp. 281–288.

[29] Y. Goldberg, A. Zakai, D. Kushnir, and Y. Ritov, "Manifold learning: The price of normalization," *Journal of Machine Learning Research*, vol. 9, pp. 1909–1939, 2008.

[30] L. Grady, "Random walks for image segmentation," *IEEE Trans. Pattern Anal. Mach. Intell.*, vol. 28, no. 11, pp. 1768–1783, Nov. 2006.

[31] G. S. Hageman and al., "An integrated hypothesis that considers drusen as biomarkers of immune-mediated processes at the RPE-bruch's membrane interface in aging and age-related macular degeneration," *Prog. Retin. Eye Res.*, vol. 20, no. 6, pp. 705–732, 2001.

[32] R. Haimovici and al., "The lipid composition of drusen, bruch's membrane, and sclera by hot stage polarizing light microscopy," *Invest. Ophthalmol. Vis. Sci.*, vol. 42, no. 7, pp. 1592–1599, 2001.

[33] A. Halevy, "Extensions of laplacian eigenmaps for manifold learning," *Ph.D. Thesis, University of Maryland*, 2011.

[34] J. Kainerstorfer, M. Ehler, and al., "Principal component model of multi spectral data for near real-time skin chromophore mapping," *J. Biomed. Opt.*, vol. 15, 2010.

[35] M. Kim and V. Pavlovic, "Covariance operator based dimensionality reduction with extension to semi-supervised settings," in *Proceedings of the 12th International Conference on Articial Intelligence and Statistics*, vol. 5, 2009.

[36] S. M. Meyers, M. A. Ostrovsky, and R. F. Bonner, "A model of spectral filtering to reduce photochemical damage in age-related macular degeneration," *Trans. Am. Ophthalmol. Soc.*, vol. 102, pp. 83–93; discussion 93–5, 2004.

[37] S. T. Roweis and L. K. Saul, "Nonlinear dimensionality reduction by locally linear embedding," *Science*, vol. 290, no. 5500, pp. 2323–2326, 2000.

[38] Z. B. Sbeh and L. D. Cohen, "A new approach of geodesic reconstruction for drusen segmentation in eye fundus images," *IEEE Trans. on Medical Imaging*, vol. 20, no. 12, pp. 1321–1333, 2001.

[39] B. Schölkopf and A. Smola, *Learning with Kernels*. Cambridge, MA: MIT Press, 2002.

[40] A. Sundaresan and R. Chellappa, "Model-driven segmentation of articulating humans in laplacian eigenspace," *IEEE Trans. Pattern Anal. Mach. Intell.*, vol. 30, no. 10, pp. 1771–85, Oct 2008.

[41] A. D. Szlam, M. Maggioni, and R. R. Coifman, "Regularization on graphs with function-adapted diffusion processes," *Journal of Machine Learning Research*, vol. 9, pp. 1711–1739, 2008.

[42] J. B. Tenenbaum, V. de Silva, and J. C. Langford, "A global geometric framework for nonlinear dimensionality reduction," *Science*, vol. 290, no. 5500, pp. 2319–23, Dec 2000.

[43] M. W. Trosset and M. Tang, "On combinatorial laplacian eigenmaps," *Technical Report, Department of Statistics, Indiana University*, 2010.

[44] U. von Luxburg, M. Belkin, and O. Bousquet, "Consistency of spectral clustering," *Ann. Stat.*, vol. 36, no. 2, pp. 555–586, 2008.

[45] L. Wang and al., "Abundant lipid and protein components of drusen," *PLoS One*, vol. 5, no. 4, p. e10329, 2010.

[46] R. C. Wilson, E. R. Hancock, and B. Luo, "Pattern vectors from algebraic graph theory," *IEEE Trans. Pattern Anal. Mach. Intell.*, vol. 27, no. 7, pp. 1112–24, Jul 2005.

[47] W. H. Wolberg and O. L. Mangasarian, "Multisurface method of pattern separation applied to breast cytology diagnosis," *Proceedings of the National Academy of Sciences*, vol. 87, pp. 9193–9196, 1990.

[48] B. Zeeberg and al., "GoMiner: A resource for biological interpretation of genomic and proteomic data," *Genome Biology*, vol. 4, no. 4, 2003.

[49] X. Zhu, Z. Ghahramani, and J. Lafferty, "Semi-supervised learning using gaussian fields and harmonic functions," *Proc. of the ICML*, 2003.